Cell Host & Microbe
Article

An Iron-Containing Dodecameric Heptosyltransferase Family Modifies Bacterial Autotransporters in Pathogenesis

Qiuhe Lu,[1,8] Qing Yao,[1,8] Yue Xu,[1,2,8] Lin Li,[1] Shan Li,[1] Yanhua Liu,[3] Wenqing Gao,[1] Miao Niu,[1] Michal Sharon,[4] Gili Ben-Nissan,[4] Alla Zamyatina,[5] Xiaoyun Liu,[3] She Chen,[1] and Feng Shao[1,6,7,*]
[1]National Institute of Biological Sciences, Beijing 102206, China
[2]College of Biological Sciences, China Agricultural University, Beijing 100094, China
[3]Institute of Analytical Chemistry & Synthetic and Functional Biomolecules Center, College of Chemistry and Molecular Engineering, Peking University, Beijing 100871, China
[4]Department of Biological Chemistry, The Weizmann Institute of Science, Rehovot 76100, Israel
[5]Department of Chemistry, University of Natural Resources and Life Sciences, A-1190 Vienna, Austria
[6]National Laboratory of Biomacromolecules, Institute of Biophysics, Chinese Academy of Sciences, Beijing 100101, China
[7]National Institute of Biological Sciences, Beijing, Collaborative Innovation Center for Cancer Medicine, Beijing 102206, China
[8]Co-first author
*Correspondence: shaofeng@nibs.ac.cn
http://dx.doi.org/10.1016/j.chom.2014.08.008

SUMMARY

Autotransporters deliver virulence factors to the bacterial surface by translocating an effector passenger domain through a membrane-anchored barrel structure. Although passenger domains are diverse, those found in enteric bacteria autotransporters, including AIDA-I in diffusely adhering *Escherichia coli* (DAEC) and TibA in enterotoxigenic *E. coli*, are commonly glycosylated. We show that AIDA-I is heptosylated within the bacterial cytoplasm by autotransporter adhesin heptosyltransferase (AAH) and its paralogue AAH2. AIDA-I heptosylation determines DAEC adhesion to host cells. AAH/AAH2 define a *b*acterial *a*utotransporter *h*eptosyl*t*ransferase (BAHT) family that contains ferric ion and adopts a dodecamer assembly. Structural analyses of the heptosylated TibA passenger domain reveal 35 heptose conjugates forming patterned and solenoid-like arrays on the surface of a β helix. Additionally, CARC, the AIDA-like autotransporter from *Citrobacter rodentium*, is essential for colonization in mice and requires heptosylation by its cognate BAHT. Our study establishes a bacterial glycosylation system that regulates virulence and is essential for pathogenesis.

INTRODUCTION

A common mechanism in bacterial pathogenesis is to deliver various virulence factors onto bacterial surface by the autotransporter secretion pathway (also known as type V secretion) (Dautin and Bernstein, 2007; Leyton et al., 2012). Since the IgA protease autotransporter was discovered in *Neisseria gonorrheae* (Pohlner et al., 1987), the number of autotransporters identified has expanded rapidly. All autotransporters share a similar modular structure consisting of a signal peptide, an N-terminal functional passenger domain, and a C-terminal β barrel domain that mediates translocation of the passenger domain across bacterial outer membrane. Owing to the difference in the passenger domain, diverse virulence functions, including cell adhesion and invasion, aggregation and biofilm formation, proteolytic digestion of host proteins, host cell vacuolation, and formation of bacterial actin tail, have been recorded with autotransporters from different bacterial pathogens (Benz and Schmidt, 2011; Henderson et al., 2004; Lazar Adler et al., 2011; Wells et al., 2007).

A subfamily of autotransporters, including AIDA-I from DAEC 2787 (Benz and Schmidt, 1989), TibA from enterotoxigenic *E. coli* (ETEC) H10407 (Elsinghorst and Weitz, 1994), and Ag43 from pathogenic *E. coli* species (van der Woude and Henderson, 2008), are long known to be glycosylated in their passenger domains (Benz and Schmidt, 2001; Lindenthal and Elsinghorst, 1999; Sherlock et al., 2006). The prototypical AIDA-I is proposed to mediate bacterial autoaggregation and adhesion to host cells (Benz and Schmidt, 1989; Charbonneau and Mourez, 2007; Sherlock et al., 2004). AIDA-I is widely present (Wells et al., 2010), particularly in porcine diarrheagenic *E. coli*, and has been a promising vaccine candidate (Ravi et al., 2007; Zhao et al., 2009). Glycosylation of AIDA-I and related autotransporters represents an example of protein glycosylation in bacteria (Benz and Schmidt, 2002) despite an undefined functional significance. Studies performed in the heterologous system (Benz and Schmidt, 2001; Charbonneau et al., 2012; Moormann et al., 2002) indicate the involvement of AAH in DAEC and its ETEC homolog TibC in AIDA-I and TibA glycosylation, respectively. However, AAH and TibC share little sequence homology to known glycosyltransferases, and it is not clear whether AAH/TibC harbor a glycosyltransferase activity from a biochemical perspective. Thus, how AIDA-I and related autotransporters are glycosylated and the functional significance of this modification in infection are not established.

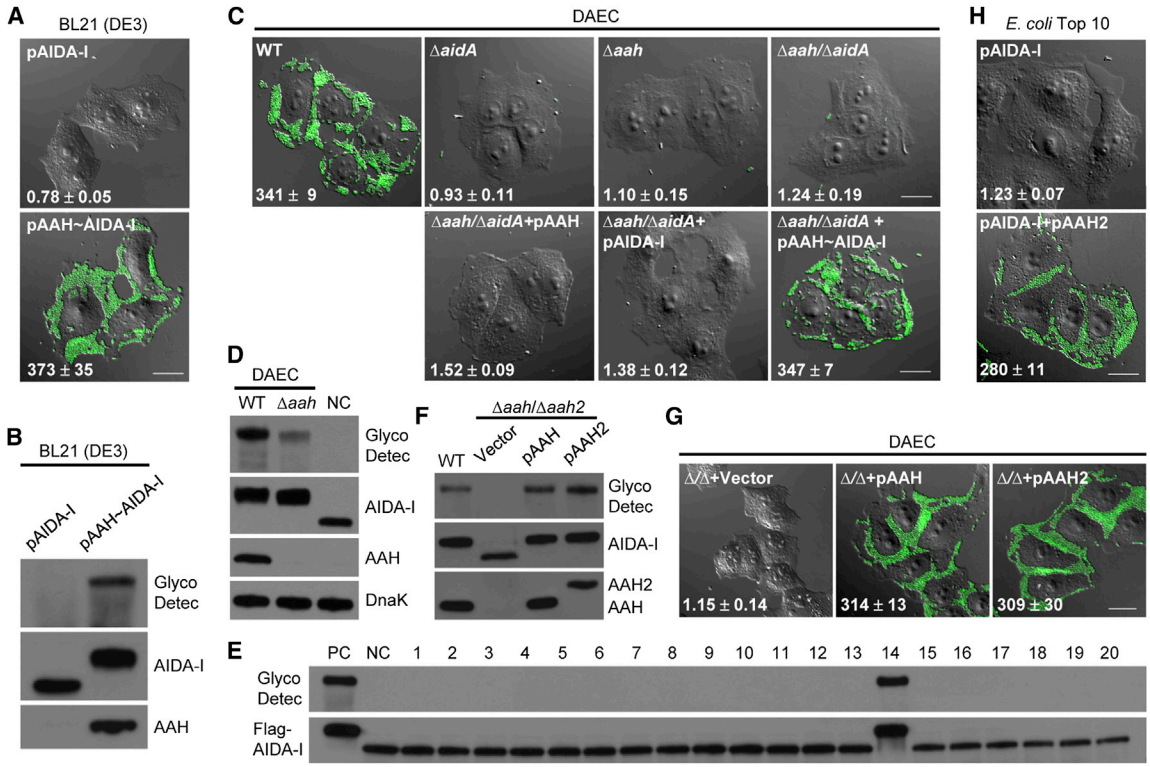

Figure 1. Glycosylation of AIDA-I Mediates DAEC Adhesion to Host Cells and Requires AAH and AAH2

(A and B) Reconstitution of AAH-induced AIDA-I glycosylation and bacterial adhesion to HeLa cells. *E. coli* BL21 (DE3) was transformed with a plasmid harboring AIDA-I alone (pAIDA-I) or the *aah-aidA* locus (pAAH∼AIDA-I). In (A), EGFP was additionally expressed to label the bacteria. Infected cells and the bacteria were visualized by differential interference contrast (DIC) microscopy and the green fluorescence, respectively. The average numbers of adherent bacteria were expressed as the mean number of bacteria adhering to one cell (the total number of recovered bacteria/the number of seeded cell in each well) ± SD of four technical repeats. Scale bar, 20 μm. In (B), bacterial lysates were subjected to anti-AIDA-I and anti-AAH immunoblotting; AIDA-I glycosylation was detected with Amersham ECL glycoprotein detection system.

(C) Genetic analyses of the *aah-aidA* locus in conferring DAEC adhesion. HeLa cells were infected with wild-type (WT) or indicated DAEC deletion strains expressing EGFP. The Δ*aah*/Δ*aidA* double deletion strain was complemented with a plasmid expressing AAH (pAAH) or AIDA-I (pAIDA-I) or both (pAAH∼AIDA-I). Data are presented similarly as in (A).

(D) Effects of *aah* deletion on endogenous AIDA-I glycosylation. Lysates of DAEC (WT or Δ*aah*) or BL21 (DE3) cells expressing AIDA-I alone (NC) were subjected to anti-AIDA-I and anti-AAH immunoblotting.

(E) Gain-of-function screen of the cryptic AIDA-I glycosyltransferase. Genomic library prepared from DAEC Δ*aah*/Δ*aidA* was introduced into *E. coli* Top10 expressing Flag-AIDA-I. Results of representative clones are shown. Lysates of Top10 cells harboring the *aah-aidA* locus and *aidA* alone serve as the positive (PC) and negative (NC) controls, respectively.

(F–H) Functional analyses of AAH2 in supporting AIDA-I glycosylation and bacterial adhesion to host cells. In (F and G), *aah/aah2* double deletion (Δ/Δ) DAEC strain was complemented with a plasmid expressing AAH or AAH2. In (H), AIDA-I (pAIDA-I) was expressed alone or together with AAH2 (pAAH2) in *E. coli* Top10. Adhesion assay in (G and H) was performed and data were presented similarly as in (A). AIDA-I glycosylation in (F) was assayed similarly as in (B).

See also Figure S1.

In this study, we provide genetic evidences that heptosylation of AIDA-I mediates DAEC adhesion to host cells, which requires AAH as well as AAH-like AAH2. In vitro biochemical analyses demonstrate that AAH and AAH2 are bone fide heptosyltransferases exclusively modifying serine residues in AIDA-I. Crystal structure of heptosylated TibA passenger domain identifies 35 heptose moieties forming patterned and solenoid-like arrays on the surface of a β helix structure. AAH and TibC define a large *b*acterial *a*utotransporter *h*eptosyl*t*ransferase (BAHT) family. We further identify an autotransporter required for *C. rodentium* colonization in infected mice, which requires hyperheptosylation by its cognate BAHT, demonstrating the importance of the BAHT family in pathogenesis.

RESULTS AND DISCUSSION

Identification of AAH2 Required for AIDA-I Glycosylation but Not for DAEC Adhesion to Host Cells

Consistent with previous studies (Benz and Schmidt, 2001; Charbonneau et al., 2012; Moormann et al., 2002), ectopic expression of the *aah-aidA* locus, but not *aidA* alone, in *E. coli* BL21 resulted in a tight adhesion of the bacteria to HeLa cells (Figure 1A) and concurrent AIDA-I glycosylation (Figure 1B). To investigate the physiological significance of these phenomena, we performed genetic analyses of the *aidA* locus. Wild-type DAEC robustly adhered to HeLa cells, and deletion of the *aah-aidA* locus completely abolished such property (Figure 1C).

Notably, deletion of *aidA* or its upstream *aah* alone also disrupted the adhesion (Figure 1C). Complementation analyses confirmed that *aidA* and *aah* were both required for DAEC adhesion to HeLa cells (Figure 1C).

Contradictory to previous understandings (Benz and Schmidt, 2001; Moormann et al., 2002), deletion of *aah* only reduced but did not completely abolish AIDA-I glycosylation (Figure 1D). This intriguing observation suggested two possibilities. AAH determines AIDA-I-mediated DAEC adhesion independently of AIDA-I glycosylation; alternatively, another cryptic glycosyltransferase accounts for the remaining AIDA-I glycosylation in DAEC Δ*aah*, but it is not sufficient to confer bacterial adhesion to host cells. Given that nonglycosylated AIDA-I could not confer adhesion of *E. coli* BL21 to HeLa cells (Figures 1A and 1B), we followed up with the latter hypothesis and attempted to identify the cryptic glycosyltransferase. The genome of DAEC 2787 has not been sequenced; a genomic library with an average insert size of 5–10 kb was prepared from the *aah*/*aidA* double deletion strain. The library plasmids were introduced into *E. coli* Top10 expressing Flag-AIDA-I. Individual recombinant was then screened for clones capable of inducing AIDA-I glycosylation. Among ~1,000 recombinants examined, clone 14 could induce AIDA-I glycosylation (Figure 1E). Sequencing of clone 14 identified a gene encoding a protein of ~75% homology to AAH (Figure S1A available online), which was named as *aah2*. Importantly, when the plasmid-born *aah* and chromosome-encoded *aah2* were both deleted, AIDA-I glycosylation in DAEC was completely abolished (Figure 1F). Anti-AAH antibody that could crossreact with overexpressed AAH2 (Figure 1F) only detected endogenous AAH, but not AAH2 (Figure 1D). The messenger RNA level of AAH2 was also much lower than that of AAH (data not shown). Thus, the low expression of endogenous AAH2 contributes to AIDA-I glycosylation but plays a negligible role in bacterial adhesion to host cells. Notably, AAH2 overexpression could restore AIDA-I glycosylation in DAEC Δ*aah*Δ*aah2* (Figures 1F and S1B) and confer AIDA-I-mediated adhesion to HeLa cells in both DAEC Δ*aah*Δ*aah2* (Figure 1G) and *E. coli* Top10 (Figure 1H). Thus, AAH2 and AAH harbor a similar biochemical function, and both of them are important for AIDA-I glycosylation. It is also a possibility that AAH2 might be involved in heptosylation of other bacterial proteins in addition to AIDA-I.

AAH/AAH2 Induce AIDA-I Hyperheptosylation on Serine Residues in the Passenger Domain

Results from above analyses and those in previous studies indicate that AAH2 and possibly also AAH may harbor a glycosyltransferase activity on AIDA-I. To identify an AIDA-I fragment that allows for testing the hypothesis in a defined in vitro system, extensive truncation analyses of AIDA-I passenger domain (residues 50–846) were performed (Figure S2A); each fragment, fused C-terminal to glutathione S-transferase (GST) and N-terminal to a Flag tag, was expressed in *E. coli* in the presence or absence of AAH. Multiple AIDA-I fragments exhibited a slow migration on the SDS-PAGE gel due to the presumed glycosylation modification (Figure S2B). The smallest one, containing residues 531–611 (AIDA-$I_{531\text{-}611}$), was further analyzed (Figure 2A). Following removal of the GST, AIDA-$I_{531\text{-}611}$-Flag was subjected to mass spectrometry analysis to unambiguously define the sugar moiety and the exact chemical linkage. Matrix-assisted laser desorption/ionization time-of-flight mass spectrometry (MALDI-TOF-MS) gave a mass of 9,867 Da that matched the theoretic mass of AIDA-$I_{531\text{-}611}$-Flag (9,866 Da) (Figure 2B). Notably, coexpression of either AAH or AAH2 resulted in a mass increase of 1,536 Da. The sample was further digested with trypsin and analyzed by liquid chromatography-tandem mass spectrometry (LC-MS/MS). Full sequence coverage was obtained, with the following peptides detected in the full-scan MS analysis: GPLGSGRPM-$_{531}$NQEGR$_{535}$ (peptide 1), $_{536}$QYVYSGATATSTVGNNEGR$_{554}$ (peptide 2), $_{555}$EYVLSGGITDGTVLNSGGLQAVSSGGK$_{581}$ (peptide 3), $_{582}$ASATVINEGGAQFVYDGGQVTGTNIK$_{607}$ (peptide 4), and $_{608}$NGGT$_{611}$-DYKDDDDK (peptide 5). In AAH/AAH2-modified samples, Peptides 1 and 4 showed a homogenous mass increase of 192 Da; peptides 2 and 3 were predominantly modified with 384 Da (2 × 192 Da) and 768 Da (4 × 192 Da), respectively, and peptide 5, containing no serine/threonine residues, was not modified. The 192 Da mass increase corresponded exactly to a heptose modification. Accordingly, the 1,536 Da mass increase on AAH/AAH2-modified AIDA-$I_{531\text{-}611}$ suggested eight heptosylation modifications.

Classical collision-induced dissociation (CID) mass spectrometry was not successful in identifying the heptosylation sites in AIDA-$I_{531\text{-}611}$-Flag due to the neutral loss during peptide fragmentation. To circumvent this problem, electron transfer dissociation (ETD) mass spectrometry that can better preserve the labile sugar moiety was employed, which identified heptosylation modifications on the two serines in peptide 2 (Figure 2C). No threonine residues in this peptide were heptosylated. All the eight serines in AIDA-$I_{531\text{-}611}$, but not any other residues, were modified according to mass spectra of other four peptides, which agreed with the total mass increase of 1,536 Da (8 × 192 Da) on AIDA-$I_{531\text{-}611}$ (Figure 2B). Thus, AAH/AAH2-induced AIDA-I heptosylation is exclusively on serine residues, a unique phenomenon in the conventional *O*-linked glycan modification.

AAH/AAH2 Induce AIDA-I Heptosylation in Bacterial Cytoplasm using ADP-Heptose from the LPS Synthesis Pathway

To investigate whether AAH/AAH2 and the heptosylation play a role in AIDA-I transport across the bacterial membrane, we first examined the subcellular localization of AAH and AIDA-I. As expected, endogenous AIDA-I was accessible to recognition by anti-AIDA-I antibody in nonpermeabilized DAEC cells (Figure S2C). Fractionation of DAEC lysates confirmed the membrane localization of AIDA-I and also revealed the cytoplasmic localization of AAH (Figure S2D). As a control, OmpA, DnaK, and Bla were enriched in the membrane, cytoplasm, and periplasm fractions, respectively. This suggests that AAHs-catalyzed AIDA-I heptosylation occurs within bacterial cytoplasm. Deletion of both *aah* and *aah2* did not affect the membrane targeting of AIDA-I (Figure S2C); AIDA-I remained enriched in the membrane fraction in the presence of a nonfunctional AAH D104A mutant in reconstituted BL21 cells (Figure S2E). Thus, AAH-catalyzed AIDA-I glycosylation is not required for surface presentation of AIDA-I. Consistent with this notion, AIDA-I is sufficient for surface display of other proteins in *aah*-deficient bacteria (Jose and Meyer, 2007).

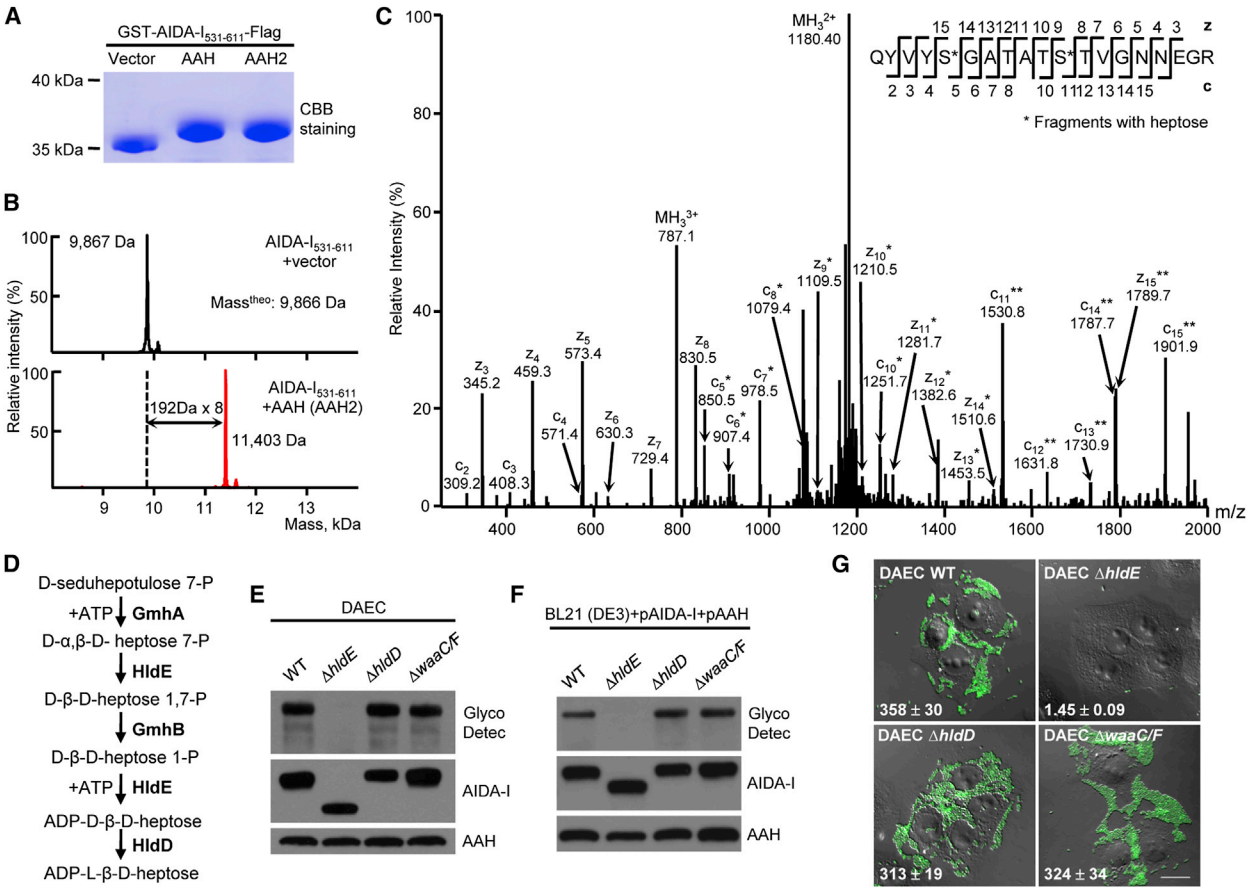

Figure 2. AAH/AAH2 Induce AIDA-I Hyperheptosylation using ADP-Heptose from the LPS Biosynsis Pathway

(A and B) SDS-PAGE and mass spectrometry analyses of GST-AIDA-$I_{531-611}$ expressed alone (vector) or coexpressed with AAH/AAH2 in *E. coli* BL21. Shown in (A) is Coomassie blue staining of purified GST-AIDA-$I_{531-611}$. The GST-removed AIDA-$I_{531-611}$ was subjected to MALDI-TOF mass spectrometry analyses in (B). The red peaks mark the glycosylated AIDA-$I_{531-611}$. AAH and AAH2 expression leads to identical mass spectra as shown.

(C) ETD-tandem mass spectrum of a triply charged tryptic peptide from AAH-modified AIDA-$I_{531-611}$. The fragmentation patterns generating the observed c and z ions are illustrated along the peptide sequence on top of the spectrum. Asterisk marks a modification on the serine by a heptose.

(D–G) Genetic analyses of the LPS synthesis pathway in AIDA-I glycosylation and DAEC adhesion. The ADP-L-β-D-heptose biosynthetic pathway in *E. coli* is illustrated in (D). Δ*hldE*, Δ*hldD*, and Δ*waaC/F* double deletion strains of DAEC or *E. coli* BL21 (DE3) were subjected to AIDA-I glycosylation (E and F) and bacterial adhesion assays (G), similarly as those in Figure 1. The average numbers of adherent bacteria on each HeLa cell are marked on the images. Scale bar, 20 μm. See also Figure S2.

Heptosylation modification has not been found on protein substrates except for AIDA-I (Benz and Schmidt, 2001). Heptosylation is only known in LPS biosynthesis, in which the sugar donors ADP-L/D-*glycero*-β-D-*manno*-heptose (ADP-L/D-D-heptose) are synthesized (Figure 2D) (Kneidinger et al., 2002). The LPS synthesis pathway has been implicated in AIDA-I glycosylation (Benz and Schmidt, 2001). In view of these observations, we constructed mutant DAEC strains deficient in *hldE* or *hldD* that encode a bifunctional kinase/adenylyltransferase and an ADP-L-glycero-D-manno-heptose-6-epimerase (Figure 2D), respectively. In Δ*hldE* where both ADP-L-D-heptose and ADP-D-D-heptose could not be synthesized, endogenous AIDA-I showed no glycosylation modification (Figure 2E). However, deletion of *hldD*, which blocked the conversion of ADP-D, D-heptose into ADP-L, D-heptose, had no such effects (Figure 2E), suggesting that ADP-D, D-heptose could serve as the sugar donor. Similar results were obtained with AIDA-I glycosylation reconstituted in *E. coli* BL21 Δ*hldE* and Δ*hldD* strains (Figure 2F). Consistently, DAEC Δ*hldE* completely lost the ability to adhere to HeLa cells while the adhesion property of Δ*hldD* was intact (Figure 2G). These in vivo data confirm that the carbohydrates linked to AIDA-I are heptose and that the sugar ligand comes from the LPS synthesis pathway.

Recombinant AAH/AAH2 Exhibit Robust Heptosyltransferase Activity

AAH is suggested to share sequence homology with LPS heptosyltransferases (Benz and Schmidt, 2001). However, our structural analyses of AAH/TibC mechanism (our unpublished data) suggest that the limited sequence similarity identified previously was likely of an accidental nature. Furthermore, deletion of *waaC* and *waaF* encoding LPS heptosyltransferase I and II (Raetz and Whitfield, 2002), respectively, did not affect AIDA-I glycosylation and DAEC adhesion to HeLa cells (Figures 2E–2G). To

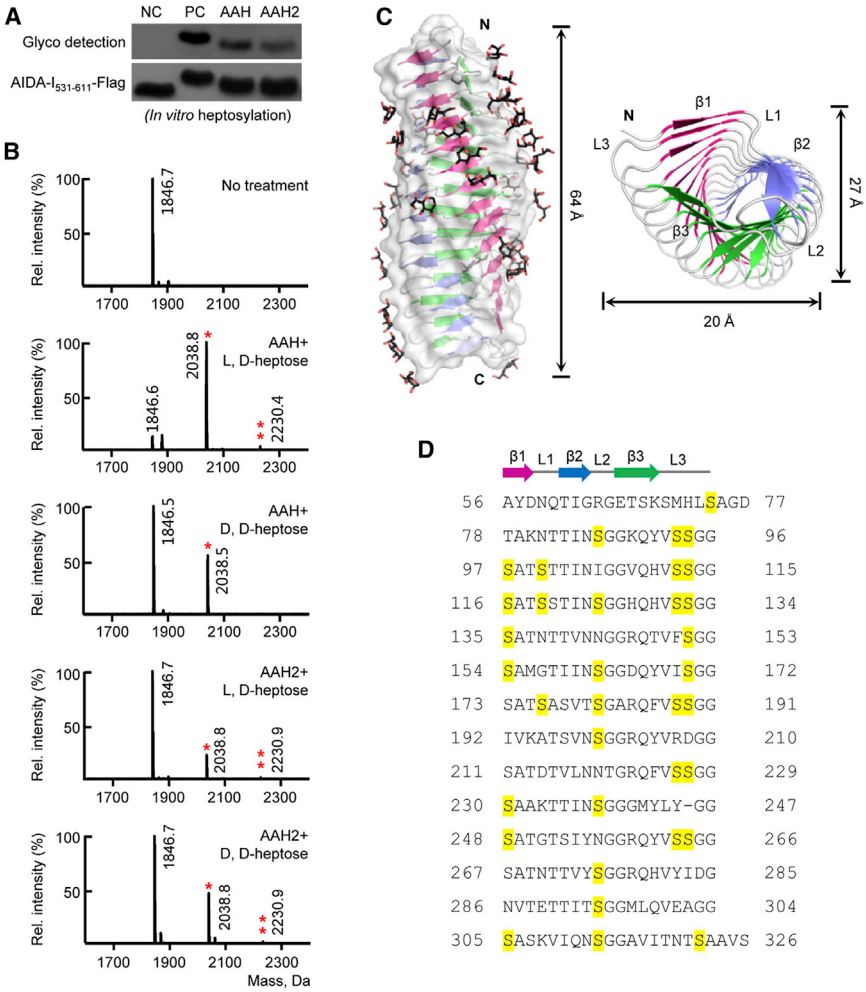

Figure 3. In Vitro Heptosyltransferase Activity of AAH/AAH2 and Crystal Structure of Hyperheptosylated TibA Passenger Domain

(A) In vitro AIDA-I heptosylation by AAH/AAH2. Purified AIDA-$I_{531-611}$-Flag was incubated with recombinant AAH or AAH2 in the presence of ADP-L, D-heptose. GST-AIDA-$I_{531-611}$-Flag coexpressed with or without AAH in *E. coli* BL21 serves as the positive (PC) and negative controls (NC), respectively.

(B) MALDI-TOF mass spectra of the TibA-derived peptide after reaction with AAH/AAH2 and ADP-L/D, D-heptose. Asterisks mark the peptides modified by one (*) or two (**) heptose molecules.

(C) The β helix structure of heptosylated $TibA_{55-350}$. The three strands are in magenta, blue, and green, respectively. TibA is in surface and ribbon diagram, and the heptoses are in black ball-and-stick models. The right shows sugar-deprived $TibA_{55-350}$.

(D) The sequence of $TibA_{55-350}$ arranged by the β-helix repeat units. Each row lists the sequence of one repeat unit, and the corresponding secondary structures are marked on top of the sequence. Glycosylated serine residues are yellow shaded. See also Figure S3 and Table S1.

definitively test whether AAH by itself harbors a heptosyltransferase activity, in vitro heptosylation was carried out. First, purified AIDA-$I_{531-611}$-Flag was efficiently glycosylated by recombinant AAH or AAH2 in the presence of synthetic ADP-L, D-heptose (Zamyatina et al., 2003) (Figure 3A). Second, four synthetic peptides derived from the passenger domains of AIDA-I and TibA were readily heptosylated by AAH, evident from the mass increase of 192 Da, and the TibA-derived peptide was the most efficient substrate (Figures 3B and S3A). Similar activity was observed with recombinant AAH2 (Figure 3B). These data provide direct and definitive evidences that AAH and AAH2 are bona fide heptosyltransferase that modify the passenger domain of AIDA-I. Consistent with genetic analyses of the LPS synthesis pathway, both ADP-L, D-heptose and ADP-D, D-heptose could support AAH and AAH2 modification of the peptide substrate (Figure 3B), indicating an absence of stereoselectivity for the sugar ligand.

Crystal Structure of Hyperheptosylated TibA Passenger Domain

While performing truncation analyses of TibC glycosylation of TibA, we identified a TibA fragment (residues 55–350) that was efficiently heptosylated by coexpressed TibC in *E. coli* BL21. Despite the insolubility of native $TibA_{55-350}$ protein, heptosylated $TibA_{55-350}$ was soluble and stable, indicating a drastic alteration of the surface property by the sugar modification. We determined the 2.1 Å crystal structure of hyperheptosylated $TibA_{55-350}$ by selenomethionine-based single-wavelength anomalous dispersion phasing (Table S1).The structure adopts a classical three-stranded right-handed β helix with an overall dimension of 20 Å × 27 Å × 64 Å (Figure 3C), similar to other structurally characterized autotransporter passenger domains (Emsley et al., 1996; Gangwer et al., 2007; Otto et al., 2005). The β helix has 14 repeat units, which are shaped into a distorted triangular prism. Each repeat unit (~19 amino acids) is similar in primary sequence and folds into three strands (β1–β3) linked by loops (L1–L3) (Figures 3C and 3D). Extensive parallel interstrand hydrogen bonds were observed at each face of the prism. A total of 35 site-specific heptose modifications were unambiguously identified from the high-quality density map (Figure 3D, and Figures S3B and S3C). Consistent with the mass spectrometry data, these heptoses are all on serine residues. Also notably, the glycosidic linkages are all in the α configuration. The heptoses are located at the beginning or end of a β strand, forming patterned and solenoid-like arrays on the β helix surface. The structure generates a vivid 3D snapshot of hyperglycosylated autotransporter passenger domain and allows for future dissecting the substrate recognition mechanism.

The Catalytic Activity of AAH Is Required for DAEC Adhesion to Host Cells

In our structure analyses of TibC (our unpublished data), Asp110 was identified as the catalytic base, and Thr226, Lys230,

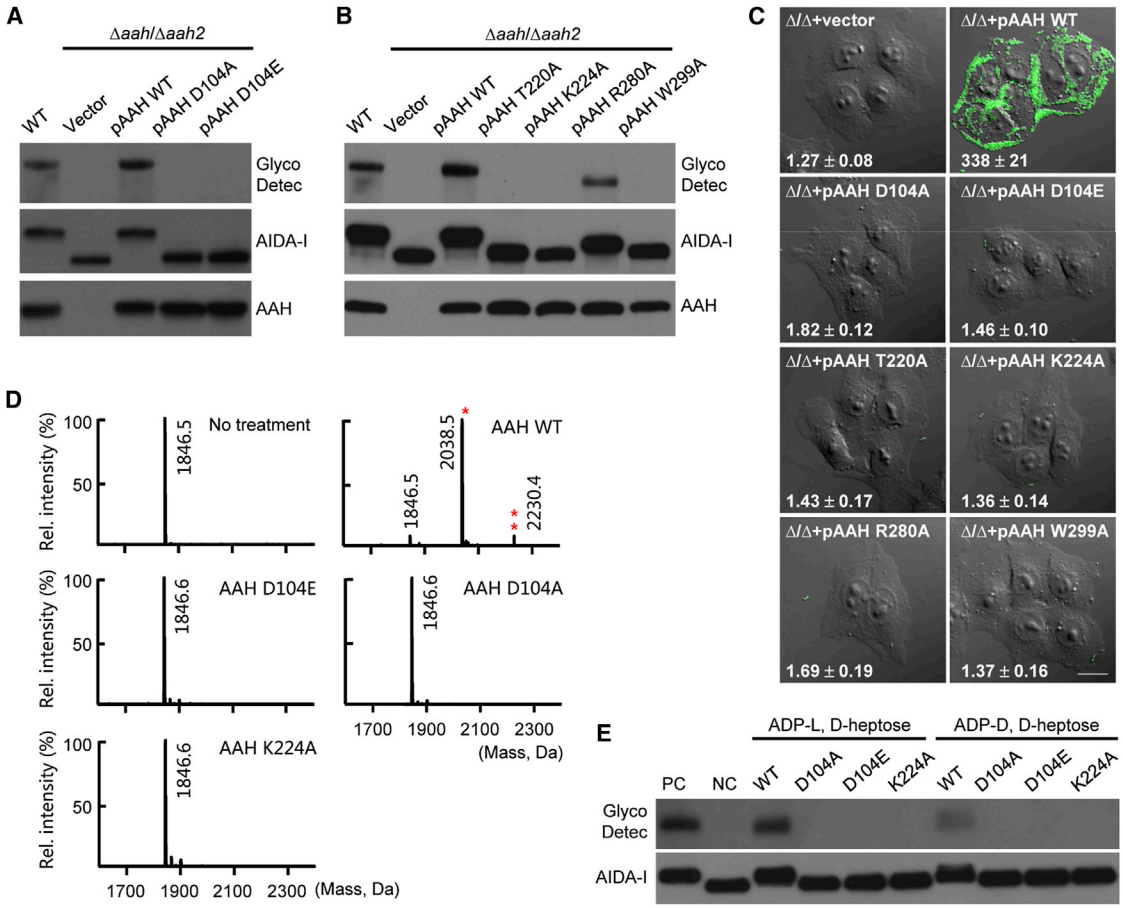

Figure 4. The Heptosyltransferase Activity of AAH Is Required for DAEC Adhesion to Host Cells

(A and B) Assays of AIDI-I glycosylation by AAH mutants in DAEC. DAEC Δ*aah*/*aah2* was complemented with a plasmid expressing wild-type (WT) or indicated AAH mutants (pAAH). AIDA-I/AAH expression and AIDA-I glycosylation were assayed as those in Figure 1B.

(C) Assays of AAH mutants in supporting DAEC adhesion to HeLa cells. DAEC *aah*/*aah2* double deletion strain (Δ/Δ) was complemented with a plasmid expressing WT or indicated AAH mutants (pAAH). Adhesion assay was performed, and data were presented similarly as in Figure 1A. Scale bar, 20 μm.

(D and E) In vitro heptosylation assays of AAH mutants using the synthetic peptide (D) and purified GST-AIDA-$I_{531-611}$ substrate (E). Shown in (D) are the MALDI-TOF mass spectra of the TibA-derived peptide following reaction with indicated AAH mutants and ADP-L, D-heptose. Asterisks mark the peptides modified by one (*) or two (**) heptose molecules. AIDA-I glycosylation was detected with Amersham ECL glycoprotein detection system in (E).

See also Figure S4.

Arg286, and Trp305 were found to be involved in binding the sugar ligand. When the equivalent catalytic base in AAH (Asp104) was replaced by an alanine or a glutamate, the mutants failed to restore AIDA-I heptosylation in DAEC Δ*aah*/Δ*aah2* (Figure 4A). Similar results were obtained with the four sugar ligand-binding site mutants despite some residual activity in AAH R280A (Figure 4B). These AAH mutants were also deficient in inducing full glycosylation of AIDA-I in *E. coli* BL21 (Figures S4A and S4B). AAH D104A, D104E, T220A, K224A, R280A, and W299A mutants, when complemented into DAEC Δ*aah*/Δ*aah2*, all failed to support AIDA-I-mediated bacterial adhesion to HeLa cells (Figure 4C). The functional deficiency of AAH R280A confirms the requirement of full glycosylation of AIDA-I for bacterial adhesion. Finally, purified AAH D104A, D104E, and K224A proteins were inactive in modifying the peptide and GST-AIDA-$I_{531-611}$ substrates (Figures 4D and 4E). These data establish the requirement of AAH heptosyltransferase activity for AIDA-I glycosylation and DAEC adhesion to host cells.

AAH Contains Iron and Adopts a Dodecamer Assembly

Purified recombinant AAH and TibC showed a brownish color (Figure 5A), suggesting the presence of a cofactor or a metal ion. Inductively coupled plasma high-resolution mass spectrometry (ICP-HRMS) unambiguously identified the presence of iron element in TibC (see below). Each AAH or TibC molecule contained one ferric ion, according to the ferrozine assay measurement (Fish, 1988) (Figure 5B). We identified two conserved cysteine residues, Cys352 and Cys364, in AAH, and mutation of either one resulted in a colorless protein. The two mutants did not glycosylate AIDA-I (Figure 5C). Mutation of a nonconserved Cys374 had no such effects. These suggest that iron binding is required for AAH glycosyltransferase activity. Moreover, purified AAH eluted as a single peak of ~450 kDa from a

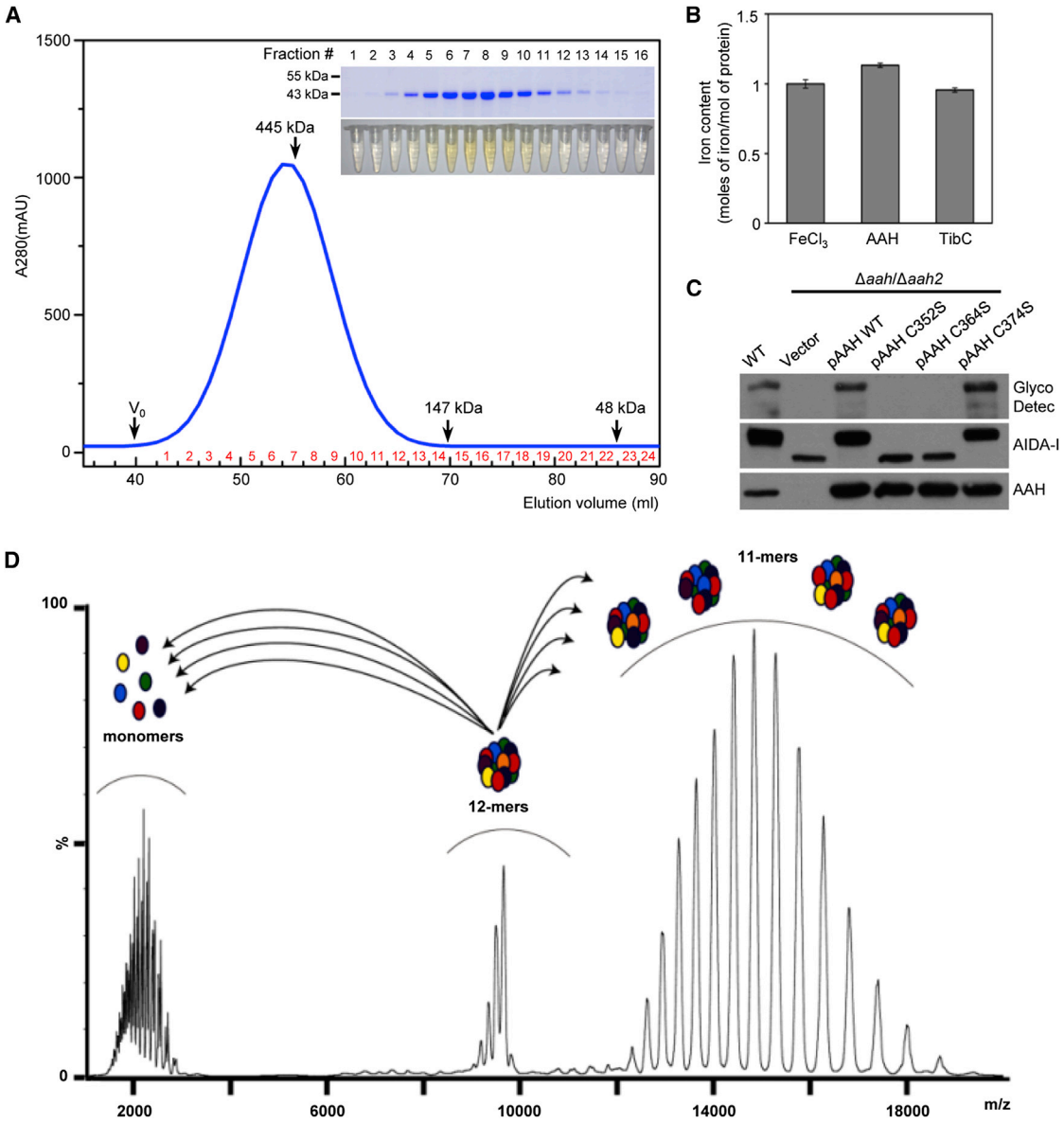

Figure 5. AAH Contains Iron and Adopts a Dodecamer Assembly

(A) Gel filtration chromatography of purified AAH on a Superdex 200 column. The red numbers mark the elution fractions. The inlet shows the color and Coomassie-stained SDS-PAGE gel of the AAH fractions.

(B) Ferrozine assay of iron contents in purified AAH and TibC. $FeCl_3$ is included as a positive control, and values are means ± SE of three technical repeats.

(C) Iron is required for AAH catalyzing AIDA-I glycosylation. DAEC *aah/aah2* was complemented with a plasmid expressing wild-type (WT) or indicated cysteine mutants of AAH (pAAH). AIDA-I/AAH expression and AIDA-I glycosylation were assayed as those in Figure 1B.

(D) Mass spectrometry analysis of the AAH oligomer. Purified AAH was subjected to nano-electrospray ionization mass spectrometry and tandem MS (MS/MS) analyses. 12-mers refer to the intact complex with a charge state series around 9,000–10,000 m/z. Monomer and 11-mers with the charge state series of around 2,000 m/z and 12,000-9,000 m/z, respectively, resulted from increasing the collision energy to 200 V.

See also Figure S5.

gel filtration column despite a predicted molecular mass of ~46 kDa. The color depth of each elution fraction correlated with elution profile of the oligomer (Figure 5A).

Nanoelectrospray ionization mass spectrometry (MS) and tandem MS (MS/MS) showed that the intact AAH oligomer appeared as a charge series centered at 9,635 m/z (ranging from 9,000 to 10,000 m/z). Under the collision energy of 200 V, the complexes were dissociated into two populations, a charge series of 12,000–19,000 m/z corresponding to the stripped complex, and the individual subunits that appeared ~2,000 m/z. (Figure 5D). Mass assignment suggested that the intact AAH oligomer contained 12 subunits. Expanding the spectrum of the monomer revealed the presence of multiple populations (Figure S5A), which correlated with the missing of N-terminal

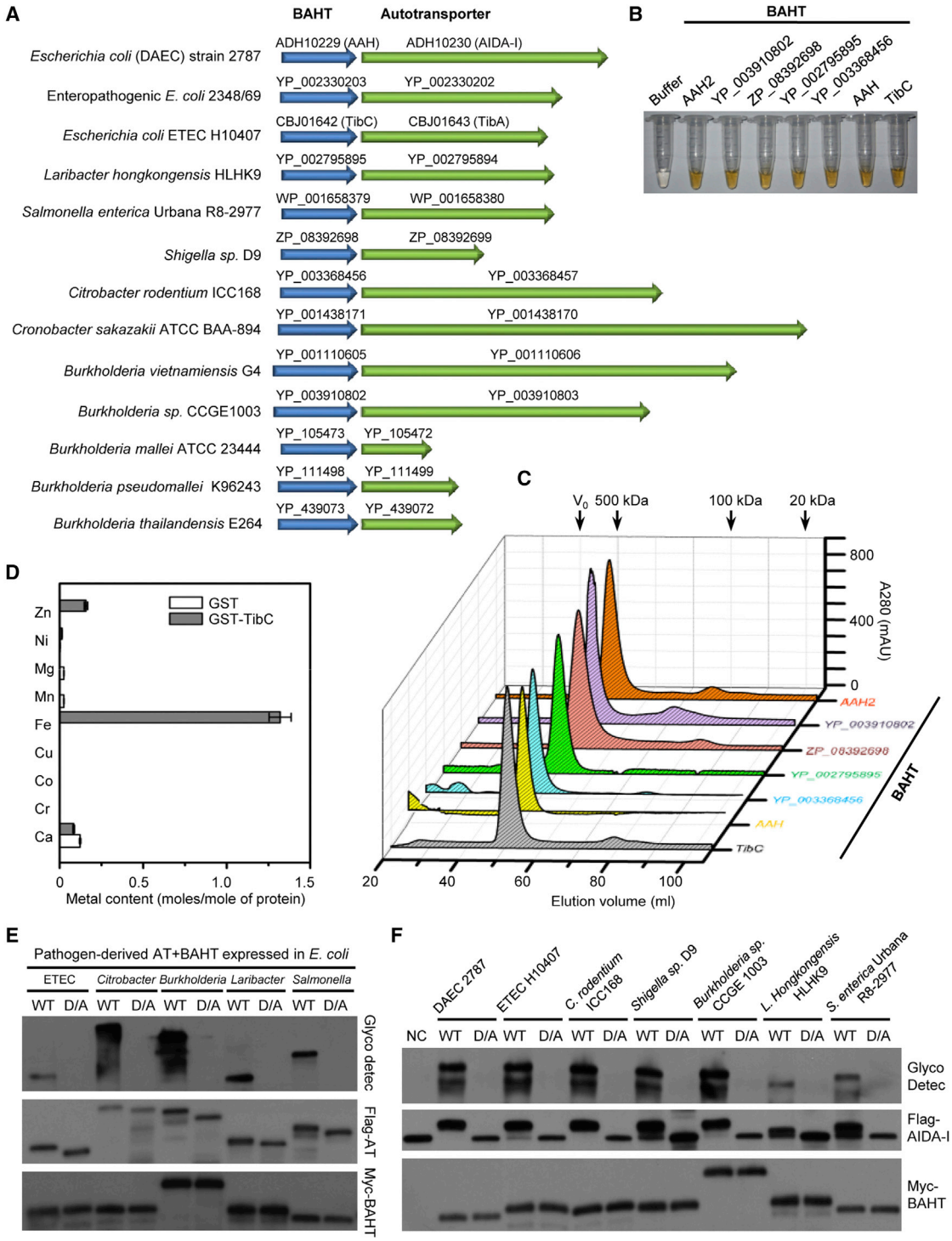

Figure 6. AAH Defines a Family of Iron-Containing Dodecameric Heptosyltransferases that Modify Their Autotransporter Partners

(A) The wide presence of BAHT family heptosyltransferases in bacteria and the corresponding genomic organization. Green and blue arrowheads indicate the BAHT family member and the autotransporter, respectively. Genbank accession numbers are marked on top of the corresponding arrowhead. The name of the bacterial strain is listed on the left of each diagram.

(B and C) The brownish color and gel filtration chromatography of purified BAHT family proteins. Recombinant AAH, AAH2, and BAHT family members from ETEC H10407 (TibC), *C. rodentium* ICC168 (YP_003368456), *Burkholderia* sp. CCGE1003 (YP_003910802), *Shigella* sp. D9 (ZP_08392698), and *L. hongkongensis* HLHK9 (YP_002795895) were purified from *E. coli* BL21 (DE3) (B) and loaded onto a Superdex 200 column (C).

(D) ICP-HRMS analysis of metal contents in purified GST and GST-TibC. Values are means ± SE of three technical repeats.

(legend continued on next page)

methionine or (partially) loss of the C-terminal 6xHis residues. The dodecamer assembly of AAH was confirmed by single particle cryoelectron microscopy (cryo-EM). In the reference-free cryo-EM micrographs, purified AAH showed clear homogeneity and a characteristic ring-like structure that could be identified in many class averages (Figure S5B). The results establish the dodecameric assembly of AAH heptosyltransferase.

AAH Defines a Family of Iron-Containing Dodecameric Heptosyltransferases Modifying Their Autotransporter Partners

AAH and TibC-like proteins are widely present in pathogenic bacteria, including but not limited to ETEC H10407, *C. rodentium* ICC168, *Salmonella enterica* serovar Urbana R8-2977, *Shigella sp.* D9, *Laribacter hongkongensis* HLHK9, *Cronobacter sakazakii* ATCC BAA-894, and several *Burkholderia* species (Figure 6A).These proteins showed ~40%–80% homology to AAH and were named as the BAHT family. Notably, nearly all *aah* homologs were immediately followed by an autotransporter or a putative autotransporter gene in the genome (Figure 6A), reminiscent of the *aah-aidA* locus in DAEC. This suggests that the BAHT family may bear similar biochemical properties as AAH and function together with their autotransporter partners. Supporting this idea, purified AAH2, TibC, and other BAHT family members from *C. rodentium* ICC168, *L. hongkongensis* HLHK9, *Shigella sp.* D9, and *Burkholderia sp.* CCGE1003 all had a brownish color (Figure 6B). These recombinant proteins all eluted as an oligomer of ~500 kDa from the gel filtration column (Figure 6C). The ICP-HRMS analyses confirmed the presence of iron (1.3 moles of irons in each mole of GST-TibC) but identified no significant amounts of other metals (Figure 6D).

When coexpressed with their partner autotransporters in *E. coli* BL21, the BAHT family members, including TibC from ETEC and those from *C. rodentium* ICC168, *Burkholderia sp.* CCGE1003, *L. hongkongensis* HLHK9, and *S. enterica* serovar Urbana R8-2977, were all capable of glycosylating their cognate autotransporters (Figure 6E). The modification was diminished by mutation of the catalytic aspartate in the BAHT. Like AAH glycosylation of AIDA-I, heptosylation of these autotransporters resulted in a slow migration on the SDS-PAGE gel (Figure 6E). These BAHT family members, when ectopically expressed in *E. coli*, could also glycosylate the coexpressed AIDA-I to various extents (Figure 6F). Despite all these similarities, we observed that ETEC H10407 and *C. rodentium* ICC168 could not compete with DAEC for adhering to HeLa cells (Figure S6A), suggesting different receptors on host cell surface targeted by the corresponding autotransporters. Finally, these BAHT family members all could heptosylate the TibA peptide in vitro (Figure S6B). Thus, BAHT is a large family of iron-containing dodecameric heptosyltransferases that targets its partner autotransporter for heptosylation.

BAHT from *C. rodentium* Glycosylates Its Partner Autotransporter, Which Is Required for Bacterial Colonization in Mice

C. rodentium is a well-established in vivo model for studying the pathogenesis of gastrointestinal pathogens. The genome of *C. rodentium* ICC168 encodes a BAHT heptosyltransferase (YP_003368456, referred to as $BAHT_{Cr}$ hereafter) that shared ~88% and 69% sequence identity to TibC and AAH, respectively (Figure 7A). $BAHT_{Cr}$ could complement AAH in restoring AIDA-I glycosylation and bacterial adhesion to HeLa cells (Figures 7B and 7C). Downstream of $baht_{Cr}$ on the chromosome was an uncharacterized gene encoding an autotransporter (YP_003368457) structurally similar to TibA and AIDA-I (Figure 7A), which was named as CARC for C. *rodentium* autotransporter required for colonization. The passenger domain of CARC consists of ~40 imperfect repeats of 19 amino acids enriched in serine residues, which is highly similar to the heptosylation motif in TibA (Figure 3D). Consistently, endogenous CARC, detected by the anti-AIDA-I antibody, was found to be glycosylated (Figure 7D). Genetic ablation of $baht_{Cr}$, confirmed by the cross-reactive recognition by the anti-TibC antibody, diminished CARC glycosylation (Figure 7D). Wild-type, but not the catalytically inactive D110A mutant of $BAHT_{Cr}$, restored CARC glycosylation in $\Delta baht_{Cr}$ (Figure 7D). Thus, $BAHT_{Cr}$ in *C. rodentium* constitutively modifies its downstream autotransporter CARC by heptosylation, reminiscent to AAH modification of AIDA-I in DAEC.

A critical early step in enteric bacterial infection is effective colonization of the gastrointestinal tract. We examined the function of $BAHT_{Cr}$ and CARC in the mouse model of *C. rodentium* infection. As expected, wild-type bacteria efficiently colonized the colon of oral-gavaged mice, demonstrated by the colony-forming units of bacteria recovered from the colons (Figure 7E). Notably, deletion of *carc* resulted in severely reduced bacterial colonization (Figure 7E). Such defects also occurred with the $\Delta baht_{Cr}$ strain (Figure 7E), which was fully rescued by wild-type but not the D110A mutant of $BAHT_{Cr}$ (Figure 7F). Thus, $BAHT_{Cr}$ heptosylation of CARC autotransporter is critical for *C. rodentium* colonization of the colons in mice.

In summary, we biochemically define the BAHT family of heptosyltransferases that are widely present in diverse pathogenic bacteria. The BAHT family members all modify their downstream autotransporter partners. BAHT has a unique dodecameric structure, with each subunit containing one ferric ion. We further show that heptosylation of *C. rodentium* CARC autotransporter by the cognate BAHT is critical for bacterial colonization of the mice, highlighting the role of an autotransporter in the colonization of this model enteropathogen.

Protein glycosylation has long been thought to be a eukaryote-specific modification but now is emerging in bacteria (Abu-Qarn et al., 2008; Nothaft and Szymanski, 2010; Szymanski and Wren, 2005). Owing to developments of new detection and isolation tools (Dube and Bertozzi, 2003), a growing number of glycoproteins of both N- and O-linked are being identified in various

(E and F) Glycosylation of the partner autotransporters and AIDA-I by several BAHT family heptosyltransferases. Flag-tagged autotransporter (AT) from indicated bacteria (E) or Flag-AIDA-I (F), together with Myc-tagged wild-type (WT) or catalytic mutant (D/A) of indicated BAHTs, were coexpressed in *E. coli* BL21 (DE3). Expression of ATs and BAHTs was detected by anti-Flag and anti-Myc immunoblotting, respectively. Glycosylation of the ATs was detected with Amersham ECL glycoprotein detection system.
See also Figure S6.

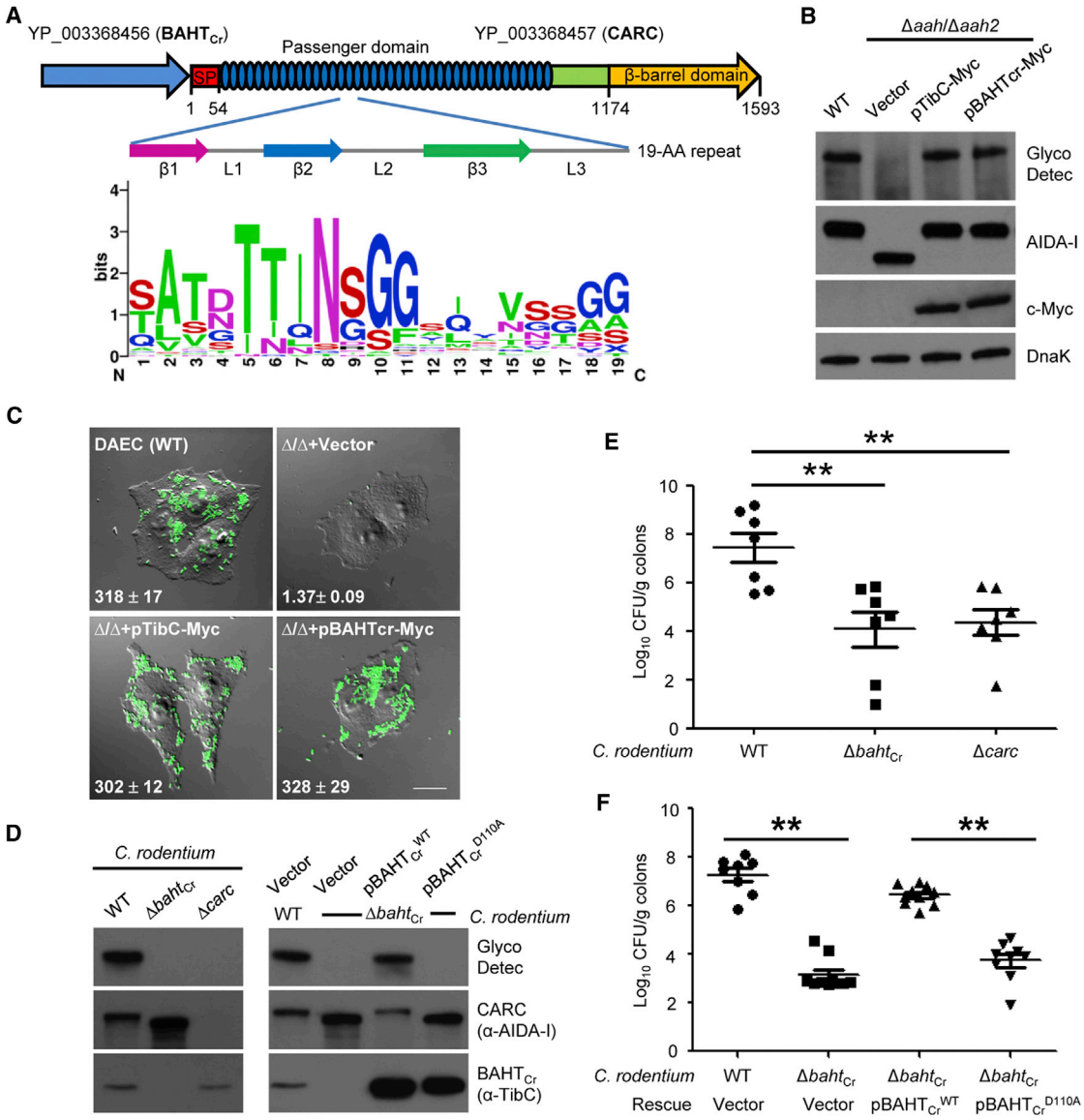

Figure 7. BAHT from *C. rodentium* Glycosylates Its Partner Autotransporter (CARC), which Is Required for Bacterial Colonization in Mice

(A) Schematic diagram of the locus of heptosyltransferase ($BAHT_{Cr}$) and the autotransporter protein (CARC) in *C. rodentium* ICC168. GenBank accession numbers for $BAHT_{Cr}$ and CARC are marked. The secondary structure (β strands, β1–β3; loops, L1–L3) and the consensus sequence of the repeat, generated by the WebLogo program (http://weblogo.berkeley.edu/) are illustrated as shown.

(B and C) Assays of $BAHT_{Cr}$ in supporting AIDA-I glycosylation and DAEC adhesion to HeLa cells. DAEC Δ*aah*/Δ*aah2* (Δ/Δ) was transformed with a vector or a plasmid expressing C-terminal Myc-tagged TibC or $BAHT_{Cr}$. The assays were performed and data are presented similarly as in Figure 1. Scale bar, 20 μm.

(D) Genetic analyses of $BAHT_{Cr}$ modification of CARC in *C. rodentium*. Lysates of indicated *C. rodentium* ICC168 strains were subjected to anti-AIDA-I and anti-TibC immunoblotting to detect CARC and $BAHT_{Cr}$ expression, respectively. CARC glycosylation was detected with the ECL glycoprotein detection system.

(E and F) Effects of $baht_{Cr}$ or *carc* deletion or loss of $BAHT_{Cr}$ heptosyltransferase activity on *C. rodentium* colonization in mice. Five- to six-week-old C57BL/6 mice were oral gavaged with wild-type (WT) or indicated deletion/complementation strains of *C. rodentium* ICC168. Bacterial colonization of the intestine 8 days after infection is shown as the mean ± SEM of $\log_{10}$ CFU/g colon ($n > 7$). The p value for the Student's t test was calculated (**$p < 0.01$).

bacteria (Longwell and Dube, 2013), many of which function in bacterial pathogenesis and immune evasion (Dube et al., 2011; Fletcher et al., 2009). Identification of the unique heptosylation system mediated by the BAHT family will significantly advance future studies on bacterial glycosylation. Moreover, given the diverse and important functions of bacterial autotransporters, the finding that heptosylation of AIDA-I and related autotransporters is required for their functioning in the host rather than in the bacteria shall also help to better understand the virulence mechanism of these bacterial autotransporter prototypes.

EXPERIMENTAL PROCEDURES

Bacteria, Plasmids, Antibodies, and Reagents

DAEC 2787 and *C. rodentium* ICC168 were provided by Dr. John M. Fairbrother (The Université de Montréal, Canada) and Dr. Youcun Qian (Institute of Health Sciences, Chinese Academy of Sciences, China), respectively. Other *E. coli* strains used include Top10 for molecular cloning, BL21 (DE3) for protein expression and glycosylation reconstitution, and SM10 (λ pir) for plasmid conjugal transfer. Bacterial deletion mutants were generated by homologous recombination as described previously (Li et al., 2013). For complementation of DAEC mutants, DNAs for AAH/AAH2, together with the respective promoter, were inserted into the pBluescript II SK (+) vector; the coding sequence of AIDA-I (fused to the promoter of *aah*) or the entire *aah-aidA* locus (including the promoter) was constructed into the EZ-T vector. For complementation in *C. rodentium* ICC168, DNAs for $BAHT_{Cr}$ (together with its natural promoter) and the CARC autotransporter (fused to $BAHT_{Cr}$ promoter) were amplified by PCR and introduced into pACYC184. To assay AAH modification of AIDA-I, Flag-tagged AIDA-I fragments and AAH were cloned into pGEX-6P-2 and pACYCDuet-1, respectively. For coexpression of BAHT with its partner autotransporter (AT), the coding sequences of BAHTs and ATs from different pathogens were introduced into pET21a and pACYCDuet-1, respectively. To detect protein expression, a Myc tag was fused N terminal to the BAHT, and a Flag tag was inserted between the signal peptide and the passenger domain of the AT. Point mutations were generated by the QuikChange Site-Directed Mutagenesis Kit (Stratagene). All the plasmids were verified by DNA sequencing.

All bacterial strains were grown in Luria Bertani (LB) medium at 37°C. Concentrations of the antibiotics used are 100 μg/mL for ampicillin and streptomycin, 30 μg/mL for kanamycin, 34 μg/mL for chloramphenicol, 25 μg/mL for tetracycline, and 50 μg/mL for nalidixic acid. Anti-Flag (M2) was from Sigma; mouse anti-HA (16B12) and anti-c-Myc monoclonal antibodies (9E10) were from Covance; anti-DnaK (clone 8E2/2) was purchased from Enzo Life Sciences. Purified AAH-His_6, TibC-His_6, and GST-AIDA-I_{50-846} were used to immunize rabbits for generating polyclonal antisera. Synthetic peptides were made by Scilight Biotechnology LLC. ADP-L/D-*glycero*-β-D-*manno*-heptose were synthesized previously (Zamyatina et al., 2003). All other chemical reagents used were from Sigma unless noted.

Cell Culture and Bacterial Adhesion Assay

HeLa cells (American Type Culture Collection, ATCC) were cultured in Dulbecco's modified Eagle's medium (Thermo Scientific) supplemented with 10% fetal bovine serum (Invitrogen) at 37°C in a 5% CO_2 incubator. To monitor bacterial adhesion, cells were seeded onto glass coverslips, and 5 μl of overnight bacteria was added onto cells without centrifugation. Following 2 hr incubation (37°C in 5% CO_2), infected cells were washed to remove nonadherent bacteria and fixed with 4% paraformaldehyde. The microscopy images shown are representative of those on the entire coverslip. To quantify the adherence, HeLa cells seeded in 24-well plates (1.2×10^5 cells/well) were used, and infected cells were lysed (0.1% Triton X-100 in PBS) to liberate the adherent bacteria. The lysates were plated on LB agar with specific antibiotics to enumerate the adherent bacteria. The results were expressed as the mean number of bacteria adhering to one cell (the total number of recovered bacteria/the number of seeded cell in each well) ± SD of four technical repeats. All experiments were independently repeated more than three times.

Immunoblotting and Glycoprotein Detection

Of 100 μl total lysates from 1 ml of bacteria culture, 1/10 was separated on SDS-PAGE gels for immunoblotting analysis and/or glycoprotein detection. Expression of AIDA-I and AAH was detected by the anti-AIDA-I and anti-AAH sera, respectively. Expression of $BAHT_{Cr}$ and the CARC autotransporter in *C. rodentium* ICC168 was monitored by anti-TibC and anti-AIDA-I immunoblotting, respectively. Glycosylation was detected with the ECL glycoprotein detection kit (GE Healthcare).

Subcellular Fractionation of Bacterial Lysates

DAEC lysates was separated into the periplasm, cytoplasm, and membrane fractions as described (Maurer et al., 1997). OmpA and β-lactamase (Bla) were expressed as the markers for outer membrane and periplamic localization, respectively. The periplasm was prepared by cold osmotic shock. Briefly, the bacteria were suspended in 50 mM Tris-HCl (pH 7.6), 20% sucrose (w/v), and 1 mM ETDA and incubated for 10 min at 4°C. The centrifuged pellets were resuspended in ice-cold 5 mM MgSO4 and incubated for another 10 min at 4°C. Following additional centrifugation, the supernatant was recovered as the periplasm fraction. The resulting pellet containing the spheroplasts was resuspended in ice-cold PBS containing a protease-inhibitor cocktail (Roche Molecular Biochemicals) and lysed by sonication. Intact spheroplasts and large debris were removed by centrifugation (12,000 g, 10 min). The supernatant was centrifuged again (100,000 g, 60 min). The final supernatant was recovered as the cytosol, and the pellet, suspended in 1% Sarkosyl (N-Lauroylsarcosine sodium salt) in PBS, was the membrane fraction (both inner and outer membranes).

Gain-of-Function Screen of *aah2* in DAEC 2787

Genomic DNA from DAEC Δ*aah*/Δ*aidA* double mutant was prepared by using TIANamp bacteria DNA Kit (TIANGEN Biotech, China). Of genomic DNA, 10 μg was digested with Sau3A1, and 5–10 kb fragments were purified from agarose gels and ligated into BamHI-digested pUC19 vector. The resulting plasmids were introduced into *E. coli* Top10 harboring pME6032-Flag-AIDA-I. The recombinants were cultured overnight with 1 mM isopropyl-β-D-thiogalactopyranoside (IPTG) to induce AIDA-I expression and then lysed for immunoblotting and glycosylation analysis.

Purification of Recombinant Proteins

E. coli BL21 (DE3) strains harboring the expression plasmids were grown in LB medium with appropriate antibiotics. Protein expression was induced by addition of 0.5 mM IPTG for 12 hr at 22°C after OD_{600} reached 0.8. Purification of His-tagged proteins was performed by using Ni-NTA agarose (GE Healthcare). GST-AIDA-I_{50-846} was expressed in the inclusion body. The inclusion bodies were solubilized in a buffer containing 6 M urea, 20 mM Tris-HCl (pH 7.6), and 20 mM NaCl; GST-AIDA-I_{50-846} was purified by the glutathione sepharose resins (GE Healthcare). Refolding of GST-AIDA-I_{50-846} was performed by dialysis against a buffer containing 20 mM Tris-HCl (pH 7.6) and 20 mM NaCl with a linear urea gradient from 6 to 0 M. GST, GST-AIDA-$I_{531-611}$-Flag, and GST-TibC were also purified by the glutathione Sepharose resins. When needed, GST was removed from the fusion protein by PreScission protease digestion. Protein concentrations were estimated by Coomassie blue staining of SDS-PAGE gels using the BSA standard.

Mass Spectrometry Analyses

To examine the AAH oligomer, nanoelectrospray ionization mass spectrometry (MS) and tandem MS (MS/MS) were performed on a QSTAR ELITE instrument. Briefly, 20 μl of the AAH complex (100 μM) was buffer exchanged into 200 mM ammonium acetate using the biospin columns (Bio-Rad). A total of 2 μl of the sample was loaded into a gold-coated nano-ESI capillary (homemade from borosilicate glass tubes). The conditions within the mass spectrometer were adjusted to preserve noncovalent interactions. The following parameters were used: capillary voltage −1.18 KV, declustering potential −150 V, focusing potential −200 V, declustering potential 2–15 V, collision energy −20 V. For tandem MS experiments, the peak centered at the m/z of 9, 635 was selected in the quadrupole and the collision energy was elevated to 200 V. Argon was used as a collision gas at the maximum pressure. Spectra are shown with minimal smoothing and without background subtraction. The mass spectrometry protocol used for determining AAH heptosylation of AIDA-I or the peptide substrate was similar to that previously described for analyzing other modifications (Li et al., 2013).

Metal Contents Determination and In Vitro Heptosyltransferase Assay

Metal contents of purified GST and GST-TibC were determined by using a Finnigan Element ICP-HRMS as described previously (Wiley et al., 2007). The iron contents of AAH-His_6 and TibC-His_6 were measured under reducing conditions by using the classical Ferrozine assay (Fish, 1988). For in vitro heptosylation, 2 μg of AAH or other purified BAHT proteins were reacted with 10 μg of AIDA-I or TibA-derived synthetic peptides for 4 hr at 30°C in a 20 μl reaction containing 10 mM Tris-HCl (pH 7.5), 50 mM NaCl, 10 mM $MgCl_2$, 1 mM DTT, and 0.5 mM ADP-L, D-heptose, or ADP-D, D-heptose. The reaction mixtures

were analyzed by mass spectrometry. To assay protein substrates, 0.5 μg of GST-AIDA-$I_{531-611}$-Flag, 0.5 μg of AAH, and 0.1 mM sugar ligand were used. The reaction mixtures were subjected to immunoblotting and glycoprotein detection analyses.

Crystallization, Data Collection, and Structure Determination

The *tibA* fragment encoding residues 55–350 was coexpressed with wild-type *tibC*. The resulting glycosylated $TibA_{55-350}$ was purified by using the Ni-NTA resin (Transgen Biotech) followed by removal of the SUMO. The protein was further purified by gel filtration chromatography and concentrated to 30 mg/mL in 10 mM Tris-HCl (pH 7.6) and 150 mM NaCl for crystallization. Crystals of native and SeMet $TibA_{55-350}$ were grown in 20% (w/v) PEG 8000, 100 mM magnesium acetate, and 100 mM Tris-HCl (pH 8.0) in 1 week. The $TibA_{55-350}$ crystals were cryoprotected with Parabar 10312 (Hampton Research) coat before flash-freezing in liquid nitrogen. The diffraction data were collected at BL-17U of Shanghai Synchrotron Radiation Facility (SSRF) at 100 K and processed with the HKL 2000 suite. The structure was solved by single-wavelength anomalous dispersion using the AutoSol-AutoBuild in PHENIX. The model was manually adjusted and completed in Coot. The final mode was refined in Refmac. Structural pictures were generated in Pymol (http://www.pymol.org/).

Mice Infection and *C. rodentium* Colonization Assays

Wild-type *C. rodentium* ICC168 and indicated derivatives were prepared by overnight shaking at 37°C. Five- to six-week-old male C57BL/6 mice were orally inoculated using a gavage needle with 200 μl bacterial suspension in PBS (~2×10^9 CFU). The number of viable bacteria used as the inoculum was determined by retrospective plating onto LB agar containing appropriate antibiotics. Eight days after inoculation, colons were removed aseptically, weighed, and homogenized in PBS. Homogenates were serially diluted and plated on MacConkey agar with proper antibiotics to determine CFU counts. *C. rodentium* colonies (pink with white rings) were counted after overnight incubation. Colonization data were analyzed using Student's t test in the software GraphPad Prism. p values <0.05 were considered significant. Independent experiments were performed using at least seven mice per group. All animal experiments were conducted following the Ministry of Health national guidelines for housing and care of laboratory animals and performed in accordance with institutional regulations after review and approval by the Institutional Animal Care and Use Committee at National Institute of Biological Sciences.

ACCESSION NUMBERS

Structural data for hyperheptosylated TibA55-350 are deposited in the Protein Data Bank (PDB) under the accession number 4Q1Q.

SUPPLEMENTAL INFORMATION

Supplemental Information includes six figures and one table and can be found with this article at http://dx.doi.org/10.1016/j.chom.2014.08.008.

AUTHOR CONTRIBUTIONS

F.S. conceived of and coordinated the study; Q.L. designed most of the experiments; Q.L., Q.Y., and Y.X. worked together and performed all the biochemical and cell culture experiments; L.L., Y.L., X.L., and S.C. performed mass spectrometry analyses of the heptosylation modification; S.L. and W.G. performed the mouse infection assay; M.S. and G.B.-N. performed mass spectrometry analysis of the AAH oligomer; M.N. and A.Z. contributed new reagents and analytic tools; Q.L. and F.S. analyzed the data and wrote the manuscript.

ACKNOWLEDGMENTS

We thank J. Fairbrother for providing DAEC 2787, J. Fleckenstein for ETEC H10407, E. Martinez for *Burkholderia sp.* CCGE1003 genomic DNA, Y. Qian for *C. rodentium* ICC168 strain, Y. Lu for *L. hongkongensis* HLHK9, and S. Roof for *S. enterica* serovar Urbana R8-2977. We thank T. Huston for ICP-HRMS analysis, F. Song and P. Zhu for cyro-EM analyses, the NIBS antibody facility for generating the antibodies, and the NIBS Biological Resource Center for gene synthesis. We also thank M. Shi for preparing the artwork, and members of the Shao laboratory for helpful discussions and technical assistance. The research was supported in part by an International Early Career Scientist grant from the Howard Hughes Medical Institute and by the Beijing Scholar Program to F.S. This work was also supported by the National Basic Research Program of China 973 Programs (2012CB518700), the Strategic Priority Research Program of the Chinese Academy of Sciences (XDB08020202), and the China National Science Foundation Program for Distinguished Young Scholars (31225002) to F.S.

Received: March 20, 2014
Revised: July 6, 2014
Accepted: August 1, 2014
Published: September 10, 2014

REFERENCES

Abu-Qarn, M., Eichler, J., and Sharon, N. (2008). Not just for Eukarya anymore: protein glycosylation in Bacteria and Archaea. Curr. Opin. Struct. Biol. *18*, 544–550.

Benz, I., and Schmidt, M.A. (1989). Cloning and expression of an adhesin (AIDA-I) involved in diffuse adherence of enteropathogenic Escherichia coli. Infect. Immun. *57*, 1506–1511.

Benz, I., and Schmidt, M.A. (2001). Glycosylation with heptose residues mediated by the aah gene product is essential for adherence of the AIDA-I adhesin. Mol. Microbiol. *40*, 1403–1413.

Benz, I., and Schmidt, M.A. (2002). Never say never again: protein glycosylation in pathogenic bacteria. Mol. Microbiol. *45*, 267–276.

Benz, I., and Schmidt, M.A. (2011). Structures and functions of autotransporter proteins in microbial pathogens. Int. J. Med. Microbiol. *301*, 461–468.

Charbonneau, M.E., and Mourez, M. (2007). Functional organization of the autotransporter adhesin involved in diffuse adherence. J. Bacteriol. *189*, 9020–9029.

Charbonneau, M.E., Côté, J.P., Haurat, M.F., Reiz, B., Crépin, S., Berthiaume, F., Dozois, C.M., Feldman, M.F., and Mourez, M. (2012). A structural motif is the recognition site for a new family of bacterial protein O-glycosyltransferases. Mol. Microbiol. *83*, 894–907.

Dautin, N., and Bernstein, H.D. (2007). Protein secretion in gram-negative bacteria via the autotransporter pathway. Annu. Rev. Microbiol. *61*, 89–112.

Dube, D.H., and Bertozzi, C.R. (2003). Metabolic oligosaccharide engineering as a tool for glycobiology. Curr. Opin. Chem. Biol. *7*, 616–625.

Dube, D.H., Champasa, K., and Wang, B. (2011). Chemical tools to discover and target bacterial glycoproteins. Chem. Commun. (Camb.) *47*, 87–101.

Elsinghorst, E.A., and Weitz, J.A. (1994). Epithelial cell invasion and adherence directed by the enterotoxigenic Escherichia coli tib locus is associated with a 104-kilodalton outer membrane protein. Infect. Immun. *62*, 3463–3471.

Emsley, P., Charles, I.G., Fairweather, N.F., and Isaacs, N.W. (1996). Structure of Bordetella pertussis virulence factor P.69 pertactin. Nature *381*, 90–92.

Fish, W.W. (1988). Rapid colorimetric micromethod for the quantitation of complexed iron in biological samples. Methods Enzymol. *158*, 357–364.

Fletcher, C.M., Coyne, M.J., Villa, O.F., Chatzidaki-Livanis, M., and Comstock, L.E. (2009). A general O-glycosylation system important to the physiology of a major human intestinal symbiont. Cell *137*, 321–331.

Gangwer, K.A., Mushrush, D.J., Stauff, D.L., Spiller, B., McClain, M.S., Cover, T.L., and Lacy, D.B. (2007). Crystal structure of the Helicobacter pylori vacuolating toxin p55 domain. Proc. Natl. Acad. Sci. USA *104*, 16293–16298.

Henderson, I.R., Navarro-Garcia, F., Desvaux, M., Fernandez, R.C., and Ala'Aldeen, D. (2004). Type V protein secretion pathway: the autotransporter story. Microbiol. Mol. Biol. Rev. *68*, 692–744.

Jose, J., and Meyer, T.F. (2007). The autodisplay story, from discovery to biotechnical and biomedical applications. Microbiol. Mol. Biol. Rev. *71*, 600–619.

Kneidinger, B., Marolda, C., Graninger, M., Zamyatina, A., McArthur, F., Kosma, P., Valvano, M.A., and Messner, P. (2002). Biosynthesis pathway of ADP-L-glycero-beta-D-manno-heptose in Escherichia coli. J. Bacteriol. *184*, 363–369.

Lazar Adler, N.R., Stevens, J.M., Stevens, M.P., and Galyov, E.E. (2011). Autotransporters and Their Role in the Virulence of Burkholderia pseudomallei and Burkholderia mallei. Front. Microbiol. *2*, 151.

Leyton, D.L., Rossiter, A.E., and Henderson, I.R. (2012). From self sufficiency to dependence: mechanisms and factors important for autotransporter biogenesis. Nat. Rev. Microbiol. *10*, 213–225.

Li, S., Zhang, L., Yao, Q., Li, L., Dong, N., Rong, J., Gao, W., Ding, X., Sun, L., Chen, X., et al. (2013). Pathogen blocks host death receptor signalling by arginine GlcNAcylation of death domains. Nature *501*, 242–246.

Lindenthal, C., and Elsinghorst, E.A. (1999). Identification of a glycoprotein produced by enterotoxigenic Escherichia coli. Infect. Immun. *67*, 4084–4091.

Longwell, S.A., and Dube, D.H. (2013). Deciphering the bacterial glycocode: recent advances in bacterial glycoproteomics. Curr. Opin. Chem. Biol. *17*, 41–48.

Maurer, J., Jose, J., and Meyer, T.F. (1997). Autodisplay: one-component system for efficient surface display and release of soluble recombinant proteins from Escherichia coli. J. Bacteriol. *179*, 794–804.

Moormann, C., Benz, I., and Schmidt, M.A. (2002). Functional substitution of the TibC protein of enterotoxigenic Escherichia coli strains for the autotransporter adhesin heptosyltransferase of the AIDA system. Infect. Immun. *70*, 2264–2270.

Nothaft, H., and Szymanski, C.M. (2010). Protein glycosylation in bacteria: sweeter than ever. Nat. Rev. Microbiol. *8*, 765–778.

Otto, B.R., Sijbrandi, R., Luirink, J., Oudega, B., Heddle, J.G., Mizutani, K., Park, S.Y., and Tame, J.R. (2005). Crystal structure of hemoglobin protease, a heme binding autotransporter protein from pathogenic Escherichia coli. J. Biol. Chem. *280*, 17339–17345.

Pohlner, J., Halter, R., Beyreuther, K., and Meyer, T.F. (1987). Gene structure and extracellular secretion of Neisseria gonorrhoeae IgA protease. Nature *325*, 458–462.

Raetz, C.R., and Whitfield, C. (2002). Lipopolysaccharide endotoxins. Annu. Rev. Biochem. *71*, 635–700.

Ravi, M., Ngeleka, M., Kim, S.H., Gyles, C., Berthiaume, F., Mourez, M., Middleton, D., and Simko, E. (2007). Contribution of AIDA-I to the pathogenicity of a porcine diarrheagenic Escherichia coli and to intestinal colonization through biofilm formation in pigs. Vet. Microbiol. *120*, 308–319.

Sherlock, O., Schembri, M.A., Reisner, A., and Klemm, P. (2004). Novel roles for the AIDA adhesin from diarrheagenic Escherichia coli: cell aggregation and biofilm formation. J. Bacteriol. *186*, 8058–8065.

Sherlock, O., Dobrindt, U., Jensen, J.B., Munk Vejborg, R., and Klemm, P. (2006). Glycosylation of the self-recognizing Escherichia coli Ag43 autotransporter protein. J. Bacteriol. *188*, 1798–1807.

Szymanski, C.M., and Wren, B.W. (2005). Protein glycosylation in bacterial mucosal pathogens. Nat. Rev. Microbiol. *3*, 225–237.

van der Woude, M.W., and Henderson, I.R. (2008). Regulation and function of Ag43 (flu). Annu. Rev. Microbiol. *62*, 153–169.

Wells, T.J., Tree, J.J., Ulett, G.C., and Schembri, M.A. (2007). Autotransporter proteins: novel targets at the bacterial cell surface. FEMS Microbiol. Lett. *274*, 163–172.

Wells, T.J., Totsika, M., and Schembri, M.A. (2010). Autotransporters of Escherichia coli: a sequence-based characterization. Microbiology *156*, 2459–2469.

Wiley, S.E., Murphy, A.N., Ross, S.A., van der Geer, P., and Dixon, J.E. (2007). MitoNEET is an iron-containing outer mitochondrial membrane protein that regulates oxidative capacity. Proc. Natl. Acad. Sci. USA *104*, 5318–5323.

Zamyatina, A., Gronow, S., Puchberger, M., Graziani, A., Hofinger, A., and Kosma, P. (2003). Efficient chemical synthesis of both anomers of ADP L-glycero- and D-glycero-D-manno-heptopyranose. Carbohydr. Res. *338*, 2571–2589.

Zhao, L., Chen, X., Xu, X., Song, G., and Liu, X. (2009). Analysis of the AIDA-I gene sequence and prevalence in Escherichia coli isolates from pigs with post-weaning diarrhoea and oedema disease. Vet. J. *180*, 124–129.